Scanning tunneling spectroscopy of single-wall carbon nanotubes on a polymerized gold substrate

F. Shao,[1] F. X. Zha,[1,*] C. B. Pan,[1] J. Shao,[2] X. L. Zhao,[1] and X. C. Shen[1,2]

[1]*Physics Department and Laboratory for Microstructures, Shanghai University, Shanghai 200444, China*

[2]*National Laboratory for Infrared Physics and Shanghai Institute of Technical Physics, Chinese Academy of Sciences, Shanghai 200083, China*

(Received 23 September 2013; revised manuscript received 28 January 2014; published 26 February 2014)

The physics picture on scanning tunneling spectroscopy of single-wall carbon nanotubes (SWCNTs) was revisited recently [H. Lin *et al*., Nat. Mater. **9**, 235 (2010)] with an image potential model under the framework of the many-body theory whose description is different from that of conventional one-particle tight-binding theory. The model is explored further in the present study of SWCNTs with an ultrahigh-vacuum scanning tunneling microscope. In the experiments, two types of samples were measured. In one sample, the nanotubes were in intimate contact with the gold surface and the observed tunneling gaps of semiconductor nanotubes fit the prediction of the one-particle model. In the other sample, the nanotubes were isolated by a thin polymer (4-vinylpyridine) layer from the gold surface. The semiconducting SWCNTs in the latter sample show tunneling gaps several hundreds of milli–electron volts larger than the prediction of the one-particle model. The results can, however, be interpreted by the modified image potential model, which takes into account the surface dielectric mechanism. The consistent picture of the tunneling gaps of the different samples provides insight into the scanning tunneling spectroscopy of SWCNTs from the standpoint of many-body theory.

DOI: 10.1103/PhysRevB.89.085423 PACS number(s): 61.48.De, 68.37.Ef, 73.22.−f

I. INTRODUCTION

Scanning tunneling microscopy (STM) and scanning tunneling spectroscopy (STS) play a unique role in characterizing the electronic properties of nanostructures. This is the most straightforward and convenient technique for the characterization of individual nanostructures in comparison with other state-of-the-art methods [1–6]. Nonetheless, to date a theoretical description of STS experiments on carbon nanotubes remains a not-well-resolved issue. Previous STS experiments on SWCNTs showed that the tunneling spectra were interpreted satisfactorily by a simple model based on the one-particle tight-binding theory [7–11]. In contrast, the many-body theory gives a very different result [6,12–15], predicting an appreciably larger band gap for a semiconductor nanotube than that predicted by the one-particle model [5]. The many-body picture has been verified by plenty of optical experiments to date [2–6]. In this context, the interpretation of STS of carbon nanotubes seems not so simple.

In most cases, a tunneling spectrum is attributed directly to the electronic structure of the freestanding nanostructure but scarcely taking into account the influence of the support substrate. STS studies on C60 and graphene revealed that the interplay between the support and the nanostructure may intensely impact the measurement of the fundamental gap [16–18]. Recent STS experiments on single-wall carbon nanotubes (SWCNTs) show that the position of the Fermi level shifts differently, depending on the substrate material [19–21]. It was pointed out that the electron screening effect of the metal substrate should not be neglected to account for the tunneling spectra [15]. The screening effect of the metal substrate was described recently with the image potential model by Lin *et al*. [22]. Their experiments showed that an SWCNT may display different tunneling gaps depending on whether the STS was measured at a position where the individual nanotube directly contacted the Au surface or at a position where the measured tube was isolated from the metal by the underlying bundle.

Although Lin *et al*.'s work casts light on the STS experiments on SWCNTs in the framework of many-body theory, further explorations of the interplay between the support substrate and the electronic structure of carbon nanotubes remain scarce until now. The present study highlights the STS characterization of SWCNTs by use of a polymerized gold surface. The polymer-treated surface introduces a different dielectric environment for carbon nanotubes so that the image potential with the tunneling is modified. It provides the ability to examine the screening effect of the support substrate. The exploration is meaningful for a comprehensive understanding of the electronic properties of carbon nanotubes, which manifest differently for optical and STS experiments.

II. EXPERIMENTAL PROCEDURE

The raw material of SWCNTs was synthesized by the arc-discharge method. For STM characterization, the pristine carbon nanotubes were ultrasonically dispersed in lithium dodecyl sulfate and purified with a centrifuge. The support substrate for nanotube deposition was a gold film evaporated on mica. The substrate was chemically modified with a 0.1 wt% solution of the polymer (4-vinylpyridine; PVP) in *N*-methylformamide, followed by rinsing with 2-propenol and air-drying. The substrate was used for nanotube adsorption by covering a drop of purified SWCNT lithium dodecyl sulfate solvent for about 25 min. The samples were then thoroughly rinsed with distilled water and dried with a stream of nitrogen. We find that the immersion time in the PVP solvent determines the PVP coverage and its thickness on the substrate. The surface is barely covered by the PVP layer with only 10 min of immersion, whereas 40 min of immersion results in a

*fxzha@shu.edu.cn

denser coverage of PVP with an average thickness of about 0.4 nm according to the STM morphology. A controlled sample (sample A) for nanotubes to be in intimate contact with the metal surface was obtained with a shorter substrate immersion time in the PVP solvent. Sample A was further heated at 180°C for 2 h in a high-vacuum chamber so as to have the least organic adsorption on the surface. In comparison, the other sample (sample B) was prepared under the condition that the substrate underwent a longer immersion time in the PVP solvent (40 min), followed by distilled water rinsing and drying in air before loading into the vacuum chamber.

The instrument is an Omicron LT scanning tunneling microscope operated at room temperature, with the base pressure generally maintained below 2.0×10^{-10} mb. An electrochemically etched tungsten tip was used for the experiments. The scope of the voltage bias and set point for imaging was generally 0.8–1.7 V and 0.02–2 nA, respectively. Current/voltage (I/V) spectra were acquired during imaging by locating the tip at any desired imaging point while the feedback loop was disabled.

III. RESULTS AND DISCUSSION

Figure 1(a) displays an image of a small SWCNT bundle with sample A. The topographic line profile across the bundle, designated by the dashed line in Fig. 1(a), is shown in Fig. 1(b). The three SWCNTs measured are labeled 1–3, respectively. The current/voltage (I/V) spectra obtained for the three nanotubes and the substrate are shown in Fig. 1(c), respectively. Note that nanotubes 1 and 2 display zero current gaps, indicating a semiconducting property, whereas nanotube 3 and the substrate display finite slopes through the $V = 0$ region, indicating a metallic property. Conventionally, the energy band gap of a semiconducting nanotube is defined by the energy interval between the first pair of van Hove singularities (VHSs) near $V = 0$ in the normalized differential spectra. However, the VHS-like spikes manifested in the spectra are likely of other origins since STM experiments have shown that electron scattering or interference with the impact of substrate or lattice defects may also lead to VHS-like features in differential spectra [21,23,24]. To avoid ambiguity, the present study focuses on discussion of the fundamental gap. Further analysis of higher energetic levels demands more delicate resolution of the dI/dV features based upon modulation technique, which is not yet accessible in the present experiment. The fundamental gap can also be estimated by a semilogarithmic plot of I/V data, in which the gap is manifested as a noise-current region whose width is easier to distinguish. To extract reliable band-gap values, we employ both the semilogarithmic plot and the numerically calculated normalized differential spectrum. As shown in Figs. 1(d) and 1(e), the band gaps for the two semiconducting nanotubes, 1 and 2, are found to be 1.07 and 0.82 eV, respectively.

Similarly to the previous STS measurements on SWCNTs [8–11], the results acquired herein can be well described by the conventional one-particle tight-binding theory [7],

$$E_{nn}^{\mathrm{TB}} = n\frac{2\gamma_0 a_{\mathrm{c\text{-}c}}}{d}, \tag{1}$$

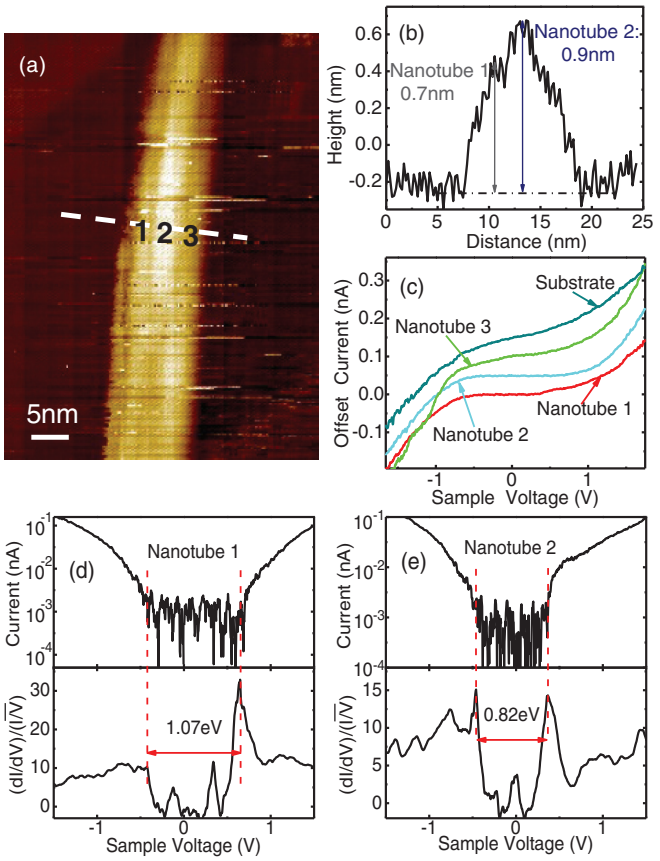

FIG. 1. (Color online) STM topography and STS of a bundle of single-walled carbon nanotubes on the Au substrate. (a) STM image of carbon nanotubes. (b) Topography line profile with respect to the white dashed line in (a). (c) Current-voltage tunneling spectra for the three nanotubes indicated in (a) and Au substrate, respectively. (d, e) Comparisons of gap measurements on the two semiconducting nanotubes, 1 and 2, by direct semilogarithmic plots of I/V and the normalized differential conductance computation.

where $a_{\mathrm{c\text{-}c}} = 0.142$ nm is the bond length of carbon-carbon atoms, d is the diameter of the carbon nanotube (in nm), and γ_0 is an empirical parameter for the hopping integral, which may take values between 2.5 and 2.9 eV [8–11]; we presently use 2.7 eV. The integer n takes the values 1,2, ..., corresponding to the energy intervals of the first, second, ... pairs of VHSs, respectively. The value of E_{11}^{TB} for $n = 1$ defines the fundamental band gap of a semiconducting nanotube. According to the height profiles shown in Fig. 1(b), the diameters of nanotubes 1 and 2 are about 0.7 and 0.9 nm. Accordingly, the band gaps calculated by Eq. (1) are 1.10 and 0.85 eV, respectively. The above calculations are in good agreement with the measured values shown in Fig. 1(d): 1.07 and 0.82 eV, respectively.

Although the one-particle theory is well supported by the above, as well as the previous, STS measurements [8–11], the appropriateness of the one-particle picture for describing the electronic structure of SWCNT was queried [15]. Numerous optical experiments to date reveal that the charge-charge interaction should not be neglected to interpret the electronic properties of carbon nanotubes [6]. However,

the inclusion of charge-charge interaction results in significant deviation of the fundamental gap from the prediction of the noninteracting one-particle model [5]. The many-body theory derives a different expression for the energy band gap (in eV) as a function of the diameter d (in nm) [5]:

$$E_{\text{gap}}^{\text{MB}} = \frac{0.34}{d} + \frac{1.11}{d+0.11}. \quad (2)$$

Equations (1) and (2) give very different band-gap values. For example, Eqs. (1) and (2) predict band gaps of a semiconducting nanotube of $d = 1$ nm to be 0.8 and 1.3 eV, respectively, indicating ~60% enlargement according to Eq. (2).

One may be curious why the STS experiments can be well interpreted by the one-particle theory, Eq. (1), rather than the many-body model, Eq. (2). Kane and Mele pointed out that the interpretation of STS measurements of SWCNTs needs to consider the electron screening effect of the metal substrate [15]. Recently, Lin *et al.* introduced the image potential modification of Eq. (2), modeling the electron screening effect of the metal substrate [22], $E_{\text{gap}}^{\text{sts}} = E_0 - C_0 e^2/2h_a$, where E_0 is the theoretical value of the band gap and h_a is the distance from the top of the nanotube to the metal surface. The coefficient C_0 is $1/4\pi\epsilon_0$ for the free-space case. Since the electric field of tunneling may induce dielectric polarization on the nanostructure as well as on the interface, the image potential energy may be reduced to a smaller value, which may be expressed as $1/(4\pi\epsilon_0\epsilon_r^{\text{eff}}) \times e^2/2h_a$, where $\epsilon_r^{\text{eff}} > 1$, representing an effective relative dielectric constant. In the work by Lin *et al.*, the image potential energy is modified by multiplying a coefficient which is actually equivalent to $1/\epsilon_r^{\text{eff}}$. Setting $C' = 1/\epsilon_r^{\text{eff}}$, we have $E_{\text{gap}}^{\text{sts}} = E_0 - C'C_0e^2/2h_a$. Replacing E_0 with Eq. (2), the above formula may be expressed in the form

$$E_{\text{gap}}^{\text{sts}} = \frac{0.34}{d} + \frac{1.11}{d+0.11} - C' \times \frac{0.72}{h_a}, \quad (3)$$

where the unit of energy is electron volts and the unit of h_a and d is nanometers. Experimentally, C' is derived through fitting Eq. (3) with the measured $E_{\text{gap}}^{\text{sts}}$ and d. In our experiment, we have $C' = 0.82$. Using the diameter values measured by the heights in Fig. 1(b), calculation by Eq. (3) gives band gaps of 1.02 and 0.82 eV for the two semiconductor nanotubes. The results calculated by Eq. (3) are in good agreement with the measured values of 1.07 and 0.82 eV as shown in Fig. 1(d). However, the value of C' (=0.82) is different that of from C' (=0.52) derived by Lin *et al.* [22]. It should be due to the fact that the latter deduced the diameter for SWCNTs using a different approach, which is the statistical analysis of the transmission electron microscopy (TEM) results [22].

In terms of TEM analysis, it is shown that the half-width of the diameter dispersion is ±0.2 nm with respect to the center of $d = 1.4$ nm [22]. Regarding the energy gap of 0.7 eV of the SWCNT which is in intimate contact with the metal, the assumption of either $d = 1.4$ nm or $d = 1.2$ nm requires different C' values to reproduce the gap, i.e., $C' = 0.52$ or 0.72, respectively. One may question whether there are also uncertainties in the height measurement. For instance, will the height measurement be influenced by the selection of imaging bias? To answer this question, we refer to data in Fig. 1. According to Fig. 1(e), the first and second VHSs for nanotube 2 should be located at $V = 0.36$ and 0.98 V. The midpoint between the first two VHSs, i.e. $V = 0.67$ V, should have a lower LDOS than the second VHS point (0.98 V). According to the I/V data in Fig. 1(c), the corresponding currents for the $V = 0.67$ and 0.98 V points are 15 and 36 pA, respectively. In comparison, the I/V for the gold surface is $I = 36$ and 63 pA with respect to the two voltages. Hence, at the lower LDOS voltage point ($V = 0.67$ V) the current ratio between the Au substrate and the nanotube is 36 pA/15 pA ≈ 2.4, whereas the ratio for the second VHS $V = 0.98$ V is 63 pA/31 pA ≈ 2.0. Assuming that the change in bias would cause a 0.1 nm difference between the gap of tip-nanotube and the gap of tip-metal, one should expect a change in the ratio of about one order. In contrast, the above ratios are almost equal, implying that the selection of either $V = 0.67$ V or $V = 0.98$ V as the imaging bias actually results in little difference in the height measurement. Practically, we did use different biases in imaging but no height difference was observed.

On the other hand, simulation based on a cylinder model shows that the so-called electronic flattening effect may cause underestimation by about 10% of the diameter in height measurement [25], namely, 0.1 nm for a $d = 1$ nm SWCNT. In fact, there are a few more factors that could influence the height measurement, including (i) tip-force-induced deformation; (ii) deformation induced by van der Waals force on the substrate; and (iii) van der Waals distance. It was observed that the tip's compression force in STM of graphite does not exceed 10 nN [26]. The AFM studies on the force interaction between tip and carbon nanotubes indicated that a tip force of 50 nN may cause ~0.5 nm compression [27,28]. Assuming that an elastic radial deformation was applied by the tip, the maximum compression by the STM tip should not exceed 0.1 nm. The surface adsorption may induce small compression, ~2% of the diameter, for an SWCNT [29]. Factor iii, the van der Waals distance, however, leads to an ~0.25-nm overestimation, which approximately cancels the sum of the other terms that lead to underestimation. In this context, the height provides a reasonable approximation for the diameter. Generally, either height measurement or TEM analysis has certain uncertainty in determining the diameter. It is worthy of further exploration to compare the difference between the two methods in determining the nanotube diameters. Regardless of their influence on C', we point out that parameter C' in either the present work or that by Lin *et al.* has been treated as an empirical value and the fractional difference between the studies does not interfere with the physics picture and main conclusions. The value of C' for the present study was derived by height measurement.

Regarding the image potential mechanism, an interesting question may be whether the tunneling gap will be modulated by the surface dielectric environment. This thought was examined with sample B, for which the nanotubes are isolated from the metal surface by a PVP layer. Figure 2(a) is the STM image of an individual SWCNT. The topographic line profile shown in Fig. 2(b) indicates that the diameter of the carbon nanotube is about 0.9 nm. The intrinsic electronic band gap of the nanotube should be 1.48 eV according to Eq. (2). With the diameter of 0.9 nm, calculation by either Eq. (1) or Eq. (3)

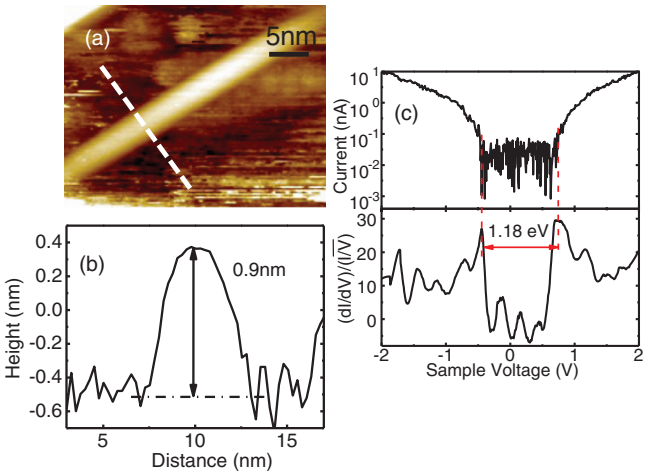

FIG. 2. (Color online) STM/STS of an individual SWCNT on a PVP-modified gold surface. (a) STM image. (b) Topography line profile for the dashed line in (a). (c) Tunneling spectra in a semilogarithm plot of I/V and normalized differential conductance.

gives results 0.85 and 1.02 eV ($C' = 0.82$ and $h_a = 1.3$ nm for Eq. (3) with the consideration of PVP thickness of about 0.4 nm), respectively. In contrast, the measured gap shown in Fig. 2(c) is 1.18 eV, whose difference from the calculations is as large as 0.33 and 0.16 eV, respectively.

One may question whether the increased band gap is related to the PVP layer. According to the roughness estimation by the surface topography profiles, the PVP layer of sample B has an average thickness of about 0.4 nm. Due to the existence of a polymer layer, it is adequate to use the double-barrier tunneling junction model to discuss the tunneling process [30]. For a small nanostructure, the measured gap will be distinctly influenced by the Coulomb charging energy E_c, which is defined as $e^2/2(C_1 + C_2)$, where C_1 and C_2 are the capacitances with the tip and the substrate, respectively [30]. Under the circumstances, the tunneling gap of a semiconducting nanostructure is contributed by both the intrinsic energy gap E_g and an additional amount, $e^2/(C_1 + C_2)$ [31]. An apparent gap also appears for a metallic nanostructure as the so-called Coulomb blockade effect. However, the Coulomb charging energy $e^2/2(C_1 + C_2)$ becomes obvious only when the capacitances are significantly low. Typically, C_1 for the vacuum barrier is about a fraction of an aF. The capacitance C_2 between the nanotube and the substrate may be calculated by the following formula according to Ref. [11],

$$C_2 = \frac{2\pi\epsilon L}{\ln((D + (D^2 - R^2)^{1/2})/R)}, \quad (4)$$

where R and L are the radius and the length of the nanotube, respectively; D is the distance from the center of the nanotube to the surface, $\epsilon = \epsilon_0\epsilon_r$, in which ϵ_0 is 8.85×10^{-3} aF/nm and $\epsilon_r = 3.5$ for PVP [32]. Assuming $D = 0.9$ nm (1-nm-diameter nanotube resting on ~0.4-nm-thick PVP) and $L = 30$ nm, calculation shows that $C_2 \sim 5.1$ aF; Hence, the enlargement of the band gap contributed by the charging effect is $\approx e^2/C_2 = 0.03$ eV. Because the SWCNTs observed in our experiment in most cases are much longer than $L = 30$ nm, which is used for the above calculation, the contribution of the charging effect is even smaller. Furthermore, we routinely observed SWCNTs with a metallic feature for sample B. The I/V spectra of those nanotubes display obvious finite slopes through $V = 0$, indicating the absence of Coulomb blockade gap.

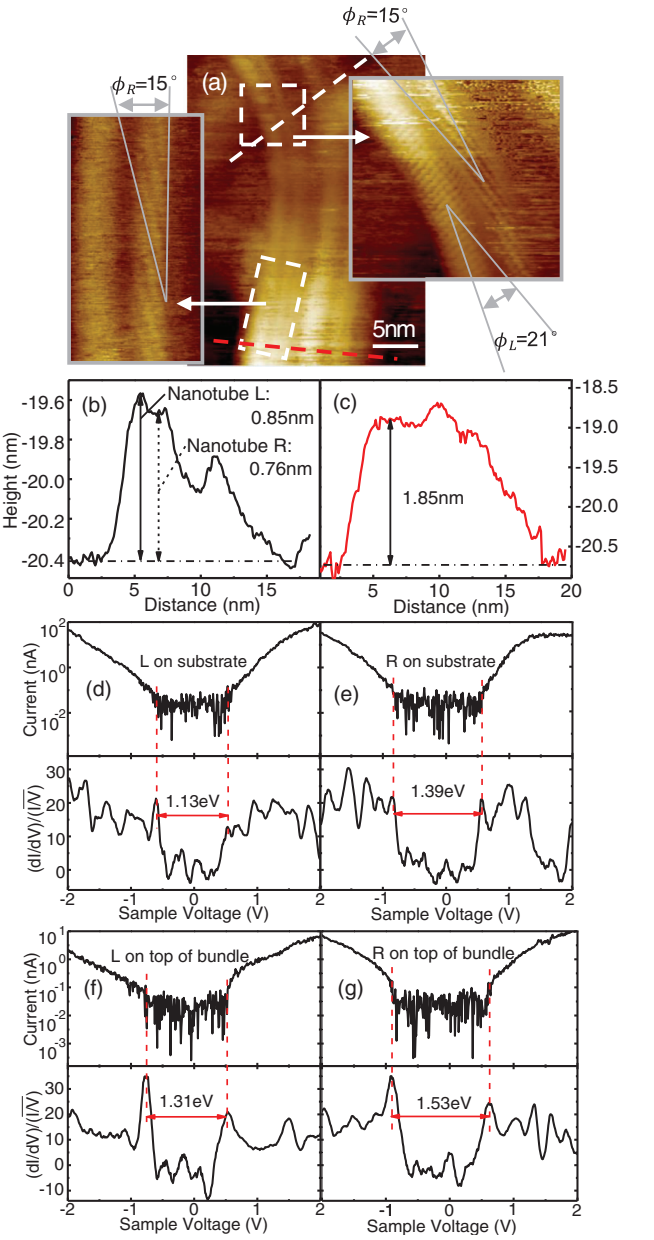

FIG. 3. (Color online) (a) STM image of an SWCNT bundle. Left and right insets: Zoom-in images with atoms resolved, corresponding to the two-frame designated location shown in the middle STM image. Two nanotubes are distinguished and labeled L (left) and R (right), respectively. Chiral angles are indicated in the insets. (b, c) Topography line profiles corresponding to white and red dashed lines in (a). (d, e) Tunneling spectra for the R and L nanotubes measured near the locations indicated by the white dashed line. (f, g) Tunneling spectra for the R and L nanotubes measured near the red-dashed-line locations.

However, we show that the PVP layer does affect the band-gap measurement through a different mechanism, addressed below. Physically, to introduce an organic layer between the nanotube and the substrate will change the dielectric environ-

ment of carbon nanotubes. The effective image potential is modified by the polarization of the organic molecules. The effect reduces the image potential and one expects a smaller value for the parameter C' than for a bare metal substrate. To deduce C' with the data in Fig. 2, we need to add the average thickness of the PVP (h_{pvp}) to the nanotube diameter (d) for h_a in Eq. (3); i.e., $h_a = d + h_{pvp} \approx 0.9 + 0.4 = 1.3$ nm. Along with the measured gap 1.18 eV in Fig. 2(c), we have $C' = 0.54$. It is reasonable that the obtained $C' = 0.54$ is smaller than that derived for the bare metal surface, $C' = 0.82$, because the dielectric polarization of PVP should reduce the image potential with a larger effective dielectric constant.

The validity and self-consistency of the above picture with the assignment of $C' = 0.54$ for the PVP-modified sample need to be examined using other experimental data. As shown in Fig. 3(a), the upper region of the image resolves two individual nanotubes, with an atomic resolution presented in the insets. Examination of the topographic line profiles indicates that the right (R) and left (L) nanotubes have heights of 0.76 and 0.85 nm, respectively. The topographic line profiles for the lower part of the bundle display approximately the same height, 1.85 nm, for the two nanotubes. The morphologies of the two nanotubes are consecutive from the upper to the lower part. Specifically, both insets display invariant helicity for the R nanotube, confirming that both the upper and the lower parts are the same tube. According to the chiral angle indicated in the insets, we deduce that the lattice indexes that match both the measured height and helicity of the R and L nanotubes should be (8, 3) and (10, 2), respectively. Starting from the derived indexes, we in turn calculate the diameters and chiral angles (d, ϕ), which are (0.77 nm, 15°) and (0.87 nm, 21°), respectively. Accordingly, we adopt the derived diameters, i.e., $d_R = 0.77$ nm and $d_L = 0.87$ nm, as the punctual values of the diameters to calculate the theoretical tunneling gaps by Eq. (3). The calculated E_{gap} for the upper and lower parts of each individual nanotube should be different because the values for h_a in Eq. (3) are different. The h_a values are obtained by adding the heights and the thickness of the PVP layer (0.4 nm). The h_a values are 1.16 and 2.25 nm for the upper and lower parts of the R nanotube and 1.25 and 2.25 nm for the upper and lower parts of the L nanotube, respectively. The measured gaps are shown in Figs. 3(c)–3(f). A comparison with the calculations is reported in Table I. One finds a good agreement between experiments and calculations using Eq. (3).

TABLE I. Comparison between STS measurements in Fig. 3 and calculated energy gaps.

Nanotube	Position	Height (nm)	Energy gap (eV)	
			Calculated by Eq. (3)	Measured
Right	In contact with substrate	1.16	1.36	1.39
	On top of bundle	2.25	1.53	1.53
Left	In contact with substrate	1.25	1.21	1.13
	On top of bundle	2.25	1.35	1.31

IV. CONCLUSION

The fundamental gaps of SWCNTs measured by STS experiments are discussed with two models, derived by the one-particle tight-binding theory and the many-body theory, respectively. Although the one-particle model well describes the tunneling gaps of nanotubes in direct contact with the gold surface, the gaps measured for SWCNTs adsorbed on the PVP-modified surface display larger values, close to the prediction of many-body theory. STS results for SWCNTs both on the bare metal surface and on the PVP layer are experimentally different but can be interpreted consistently with the image potential model in the framework of many-body theory. Since the dielectric environments for nanotubes on a bare metal surface and on a PVP layer are different, the coefficient in the image potential model should be modified with the surface conditions. This work provides a selfconsistent picture on the electronic properties of carbon nanotubes in the regime of many-body theory.

ACKNOWLEDGMENTS

This work was supported by Grant No. 91121007 of the National Science Foundation and National Basic Research Program 2011CB925601. We also thank the Shanghai Education Committee for support through academic project 085.

[1] A. Jorio, R. Saito, J. H. Hafner, C. M. Lieber, M. Hunter, T. McClure, G. Dresselhaus, and M. S. Dresselhaus, Phys. Rev. Lett. **86**, 1118 (2001).
[2] A. Malaphanis, D. A. Jones, E. Comfort, and J. U. Lee, Nano Lett. **11**, 1946 (2011).
[3] J. Maultzsch, R. Pomraenke, S. Reich, E. Chang, D. Prezzi, A. Ruini, E. Molinari, M. S. Strano, C. Thomsen, and C. Lienau, Phys. Rev. B **72**, 241402(R) (2005).
[4] F. Wang, G. Dukovic, L. E. Brus, and T. F. Heinz, Science **308**, 838 (2005).
[5] G. Dukovic, F. Wang, D. Song, M. Y. Sfeir, T. F. Heinz, and L. E. Brus, Nano Lett. **5**, 2314 (2005).
[6] M. S. Dresselhaus, G. Dresselhaus, R. Saito, and A. Jorio, Annu. Rev. Phys. Chem. **58**, 719 (2007), and references therein.
[7] R. Saito, G. Dresselhaus, and M. S. Dresselhaus, *Physical Properties of Carbon Nanotubes* (Imperial College, London, 1998).
[8] J. W. G. Wildöer, L. C. Venema, A. G. Rinzler, R. E. Smalley, and C. Dekker, Nature **391**, 59 (1998).
[9] T. W. Odom, J.-L. Huang, P. Kim, and C. M. Lieber, Nature **391**, 62 (1998).
[10] L. C. Venema, V. Meunier, Ph. Lambin, and C. Dekker, Phys. Rev. B **61**, 2991 (2000).
[11] T. W. Odom, J.-L. Huang, P. Kim, and C. M. Lieber, J. Phys. Chem. B **104**, 2794 (2000).

[12] T. Ando, J. Phys. Soc. Jpn. **66**, 1066 (1997).
[13] C. L. Kane and E. J. Mele, Phys. Rev. Lett. **90**, 207401 (2003).
[14] C. D. Spataru, S. Ismail-Beigi, L. X. Benedict, and S. G. Louie, Phys. Rev. Lett. **92**, 077402 (2004).
[15] C. L. Kane and E. J. Mele, Phys. Rev. Lett. **93**, 197402 (2004).
[16] X. Lu, M. Grobis, K. H. Khoo, S. G Louie, and M. F. Crommie, Phys. Rev. B **70**, 115418 (2004).
[17] J. D. Sau, J. B. Neaton, H. J. Choi, S. G Louie, and M. L. Cohen, Phys. Rev. Lett. **101**, 026804 (2008).
[18] S. Y. Zhou, G.-H. Gweon, A. V. Fedorov, P. N First, W. A. de Heer, D.-H. Lee, F. Guinea, A. H Castro Neto, and A. Lanzara, Nature Mater **6**, 770 (2007).
[19] S. Clair, Y. Kim, and M. Kawai, Phys. Rev. B **83**, 245422 (2011).
[20] H.-J. Shin, S. Clair, Y. Kim, and M. Kawai, Appl. Phys. Lett. **93**, 233104 (2008).
[21] H.-J. Shin, S. Clair, Y. Kim, and M. Kawai, Nature Nanotech. **4**, 567 (2009).
[22] H. Lin, J. Lagoute, V. Repain, C. Chacon, Y. Girard, J.-S. Lauret, F. Ducastelle, A. Loiseau, and S. Rousset, Nat. Mater. **9**, 235 (2010).
[23] M. Ouyang, J.-L. Huang, C. L. Cheung, and C. M. Lieber, Science **291**, 97 (2001).
[24] G. Buchs, D. Bercioux, P. Ruffieux, P. Gröning, H. Grabert, and O. Gröning, Phys. Rev. Lett. **102**, 245505 (2009).
[25] L. Tapaszto, G. I. Mark, A. Akoos, P. Lambin, and L. P. Biro, J. Phys. Condens. Matter **183**, 5793 (2006).
[26] J. M. Soler, A. M. Baro, N. Garcia, and H. Rohrer, Phys. Rev. Lett. **57**, 444 (1986).
[27] T. DeBorde, J. C. Joiner, M. R. Leyden, and E. D. Minot, Nano Lett. **8**, 3568 (2008).
[28] H. W. C. Postma, A. Sellmeijer, and C. Dekker, Adv. Mater. **12**, 1299 (2000).
[29] T. Hertel, R. E. Walkup, and P. Avouris, Phys. Rev. B **58**, 13870 (1998).
[30] A. E. Hanna and M. Tinkham, Phys. Rev. B **44**, 5919 (1991).
[31] B. Alperson, I. Rubinstein, G. Hodes, D. Porath, and O. Millo, Appl. Phys. Lett. **75**, 1751 (1999).
[32] W. Zha, C. D. Han, D. H. Lee, S. H. Han, J. K. Kim, J. H. Kang, and C. Park, Macromolecules **40**, 2109 (2007).